molbank

MDPI

Short Note

2-(*N*-allylsulfamoyl)-*N*-propylbenzamide

Ayoub El mahmoudi [1], Karim Chkirate [2], Loubna Mokhi [1], Joel T. Mague [3] and Khalid Bougrin [1,4,*]

1 Equipe de Chimie des Plantes et de Synthèse Organique et Bioorganique, URAC23, B.P. 1014, Geophysics, Natural Patrimony and Green Chemistry (GEOPAC) Research Center, Faculty of Science, Mohammed V University in Rabat, Rabat 10010, Morocco; ayoub_elmahmoudi2@um5.ac.ma (A.E.m.); loubna.mokhi@um5r.ac.ma (L.M.)
2 Laboratory of Heterocyclic Organic Chemistry URAC 21, Pharmacochemistry Competence Center, Av. Ibn Battouta, B.P. 1014, Faculty of Sciences, Mohammed V University in Rabat, Rabat 10010, Morocco; k.chkirate@um5r.ac.ma
3 Department of Chemistry, Tulane University, New Orleans, LA 70118, USA; joelt@tulane.edu
4 Chemical & Biochemical Sciences Green-Process Engineering (CBS), Mohammed VI Polytechnic University, Lot 660, Hay Moulay Rachid, Ben Guerir 43150, Morocco
* Correspondence: k.bougrin@um5r.ac.ma

Abstract: In this work, a new compound, 2-(*N*-allylsulfamoyl)-*N*-propylbenzamide, has been synthesized via a tandem *one-pot* reaction under sonication. The rotational orientations of the allylsulfamoyl and the amide groups in the title molecule, $C_{13}H_{18}N_2O_3S$, are partly determined by an intramolecular N—H···O hydrogen bond. In the crystal, a layer structure is generated by N—H···O and C—H···O hydrogen bonds plus C—H···π (ring) interactions. A Hirshfeld surface analysis indicates that the most important contributions to crystal packing are from H···H (59.2%), H···O/O···H (23.5%), and H···C/C···H (14.6%) interactions. The optimized structure calculated using density functional theory at the B3LYP/6–311 G (d,p) level is compared with the experimentally determined structure in the solid state. The calculated highest occupied molecular orbital (HOMO) and lowest unoccupied molecular orbital (LUMO) energy gap is 5.3828 eV.

Keywords: crystal structure; DFT; secondary sulfonamide; hydrogen bond; Hirshfeld surface analysis; ultrasound cavitation

check for updates

Citation: El mahmoudi, A.; Chkirate, K.; Mokhi, L.; Mague, J.T.; Bougrin, K. 2-(*N*-allylsulfamoyl)-*N*-propylbenzamide. *Molbank* **2023**, *2023*, M1678. https://doi.org/10.3390/M1678

Academic Editors: Antonio Salomone and Serena Perrone

Received: 24 May 2023
Revised: 25 June 2023
Accepted: 27 June 2023
Published: 30 June 2023

1. Introduction

Sulfonamides are a very interesting class of drugs because of their many pharmacological properties [1], including their ability to inhibit carbonic anhydrase "CA" and their diuretic [2,3], anticancer [4], hypoglycemic [5], antiviral [6], antibacterial [7], and metalloprotease inhibitory effects [8]. Although they were discovered in the 1930s as chemotherapeutic agents for their antibacterial properties, they have recently attracted increasing interest due to the discovery of new pharmacological properties [9]. Recent studies have shown that secondary sulfonamides have significant potential, not only for their ability to selectively inhibit "CA" isozymes but also for their beneficial properties in the treatment of cancer and for glutamate carboxypeptidase II inhibition [10].

The reaction that combines amino compounds with sulfonyl chlorides is the most common method for synthesizing secondary sulfonamide derivatives. This method requires difficult synthetic conditions, multiple steps, and long reaction times and results in the production of undesirable chemicals and toxic byproducts [11]. Therefore, finding a green and efficient source for the synthesis of secondary sulfonamide derivatives should be a priority. Our research group has recently developed the synthesis of a new series of heterocyclic units bearing secondary sulfonamides using an eco-friendly protocol under ultrasound cavitation [12,13].

Theoretical calculations, besides measuring the activity of molecules, give important information about many properties of these molecules [14]. Owing to the wide range of applications mentioned above, the title compound 2-(*N*-allylsulfamoyl)-*N*-propylbenzamide

was synthesized and characterized spectroscopically. The three-dimensional structure was determined by a single-crystal X-ray diffraction analysis. The intermolecular interactions and the hydrogen bonds were studied by a Hirshfeld surface analysis and supplemented by density functional theory (DFT) calculations to establish the optimized molecular structural parameters of the compound, HOMO–LUMO energies, and thermodynamic parameters. The chemical properties of the molecule were investigated using Gaussian calculations, applying B3LYP methods with the 6–311 g(d,p) basis set.

2. Results

2.1. Synthesis

We started our *one pot* three-component tandem reaction with the *N*-allylation reaction using saccharin **1** (1 equivalent), allyl bromide **2** (1.1 equivalents) and K_2CO_3 (1.2 equivalents) as a base in water as the solvent under ultrasonic cavitation at 25 °C. The reaction was completed in a very short time and monitored by thin-layer chromatography (TLC) to confirm the formation of *N*-allyl saccharin as the expected intermediate. This compound was then reacted in situ with propylamine **3** (2 equivalents) to give 2-(*N*-allylsulfamoyl)-*N*-propylbenzamide **4** by intermolecular N-C-σ-saccharin ring cleavage under ultrasonic cavitation. The reaction exhibited an excellent yield, with 94% of the desired product **4** (Scheme 1). The structure of **4** was fully characterized by IR, ^{13}C, ^{1}H NMR, and LCMS spectra, and confirmed by single-crystal X-ray diffraction.

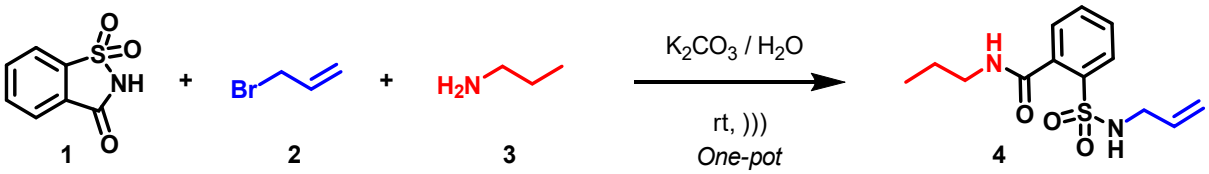

Scheme 1. Synthesis of compound **4**.

2.2. Crystal Structure Determination

The crystal was kept at 150(2) K during data collection which proceeded under control by APEX4 [15] software. The structure was solved with the SHELXT [16] structure solution program using Intrinsic Phasing and refined with the SHELXL [17] refinement package using full-matrix, least-squares methods. 2-(*N*-allylsulfamoyl)-*N*-propylbenzamide crystallizes in the monoclinic space group P21/c with one molecule in the asymmetric unit (Figure 1).

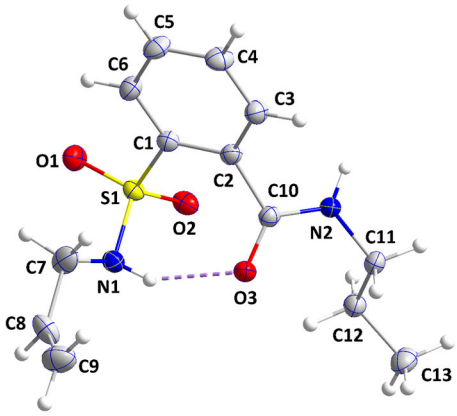

Figure 1. The title molecule with labeling scheme and 50% probability ellipsoids. An intramolecular hydrogen bond is depicted by a dashed line. Only the major component of the disorder is shown.

The rotational orientations of the two substituents on the C1⋯C6 ring are partly determined by the intramolecular N1---H1⋯O3 hydrogen bond (Table 1 and Figure 2). These orientations can be appreciated by the C1---C2---C10---O3 and C2---C1---S1---N1

torsion angles which are, respectively, −56.67 (16) and 72.94 (10)°. The sum of the angles about N2 is 360 (1)°, indicating participation of the lone pair in N-C···π bonding. This is largely with C10 (N2-C10 = 1.3335(15) Å) because of the presence of the carbonyl group. In the crystal, inversion dimers are generated by N2---H2A···O2 hydrogen bonds and C12---H12A···Cg1 interactions (Table 1 and Figure 2). With the major orientation of the disordered allyl group constituting 92% of positions of this group throughout the crystal, the great majority of the packing can be described as the dimers being connected by C9---H9B···O4 hydrogen bonds (Table 2) to form layers of molecules parallel to (204) (Figure 2). The layers are stacked along the direction of the normal to (204) (Figure 3).

Table 1. Hydrogen bond geometry (Å, °) for 2-(*N*-allylsulfamoyl)-*N*-propylbenzamide. Cg1 is the centroid of the C1···C6 benzene ring.

D*—H···*A	***D*—H**	**H···*A***	**D···*A***	***D*—H···*A***
N1—H1···O3	0.853 (18)	2.108 (18)	2.8759 (14)	149.5 (15)
N2—H2A···O2 [i]	0.855 (16)	2.175 (16)	2.9818 (13)	157.4 (14)
C9—H9B···O1 [ii]	0.95	2.55	3.480 (6)	165
C12—H12A···Cg1 [i]	0.99	2.76	3.6902 (15)	156

Symmetry codes: (i) $-x+2, -y+1, -z+1$; (ii) $x-1, -y+3/2, z-1/2$.

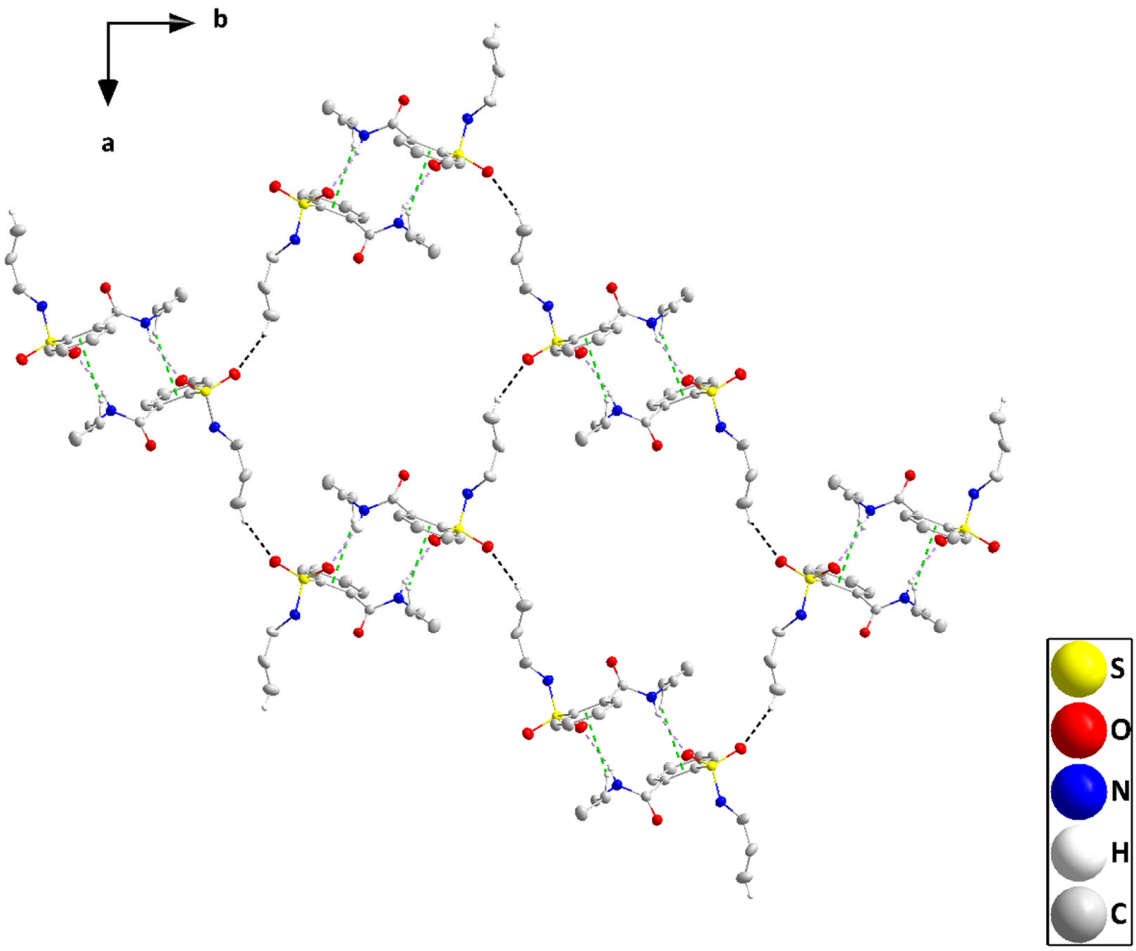

Figure 2. A portion of one layer viewed along the c-axis with N—H···O and C—H···O hydrogen bonds depicted, respectively, by violet and black dashed lines. The C—H···π(ring) interactions are depicted by green dashed lines and non-interacting hydrogen atoms are omitted for clarity.

Table 2. Comparison (X-ray and density functional theory) of selected bond lengths and angles (Å, °).

	X-ray	B3LYP/6–311 G(d,p)
S1-N1	1.6238 (10)	1.6711
S1-C1	1.7769 (11)	1.8111
S1-O1	1.4327 (9)	1.4619
N1-C7	1.4816 (16)	1.4674
C10-O3	1.2353 (14)	1.2265
C10-N2	1.3335 (15)	1.3557
N2-C11	1.4614 (14)	1.4616
S1-O2	1.4382 (8)	1.4651
C1-S1-O1	107.19 (5)	108.2414
O1-S1-N1	107.83 (5)	106.6917
S1-N1-C7	116.25 (9)	118.1819
N1-C7-C8	108.95 (13)	111.869
C6-C1-S1	118.00 (9)	116.7889
C2-C1-S1	121.07 (8)	121.8659
C2-C10-O3	120.14 (10)	121.6204
C2-C10-N2	116.03 (10)	114.9641
C10-N2-C11	121.61 (10)	121.9677
N2-C11-C12	113.69 (10)	113.0569
C1-S1-O2	107.73 (5)	106.7981
O3-C10-N2	123.75 (10)	123.3388

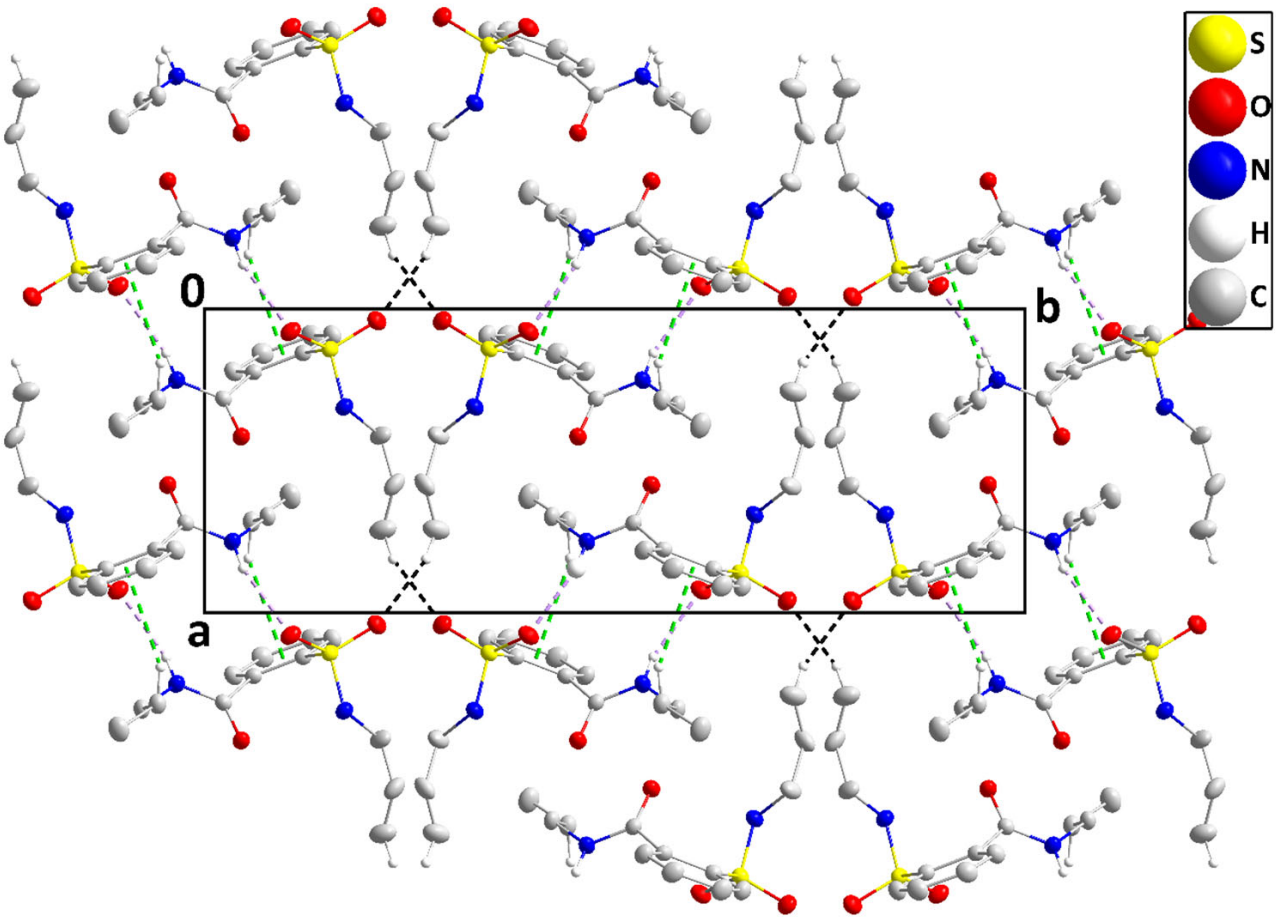

Figure 3. Packing viewed along the c-axis with intermolecular interactions depicted as in Figure 2 and non-interacting hydrogen atoms omitted for clarity.

To visualize the intermolecular interactions of 2-(*N*-allylsulfamoyl)-*N*-propylbenzamide, a Hirshfeld surface (HS) analysis [18,19] was carried out by using Crystal Explorer 17.5 [20]. In the HS plotted over d_{norm} (Figure 4a), the white surface indicates contacts with distances equal to the sum of van der Waals radii, and the red and blue colors indicate distances shorter (in close contact) or longer (distant contact) than the van der Waals radii, respectively. The most important red spots and the corresponding interactions are shown in Figure 5. The shape index (Figure 4b) generated in the range of −1 to 1 Å reveals that there are no π–π interactions, normally indicated by adjacent red and blue triangles. The electrostatic potential using the STO-3G basis set at the Hartree–Fock level of theory and mapped on the Hirshfeld surface over the range of ±0.05 a.u. clearly shows the positions of close intermolecular contacts in the compound (Figure 4c). The positive electrostatic potential (blue region) over the surface indicates hydrogen donor potential, whereas the hydrogen bond acceptors are represented by a negative electrostatic potential (red region).

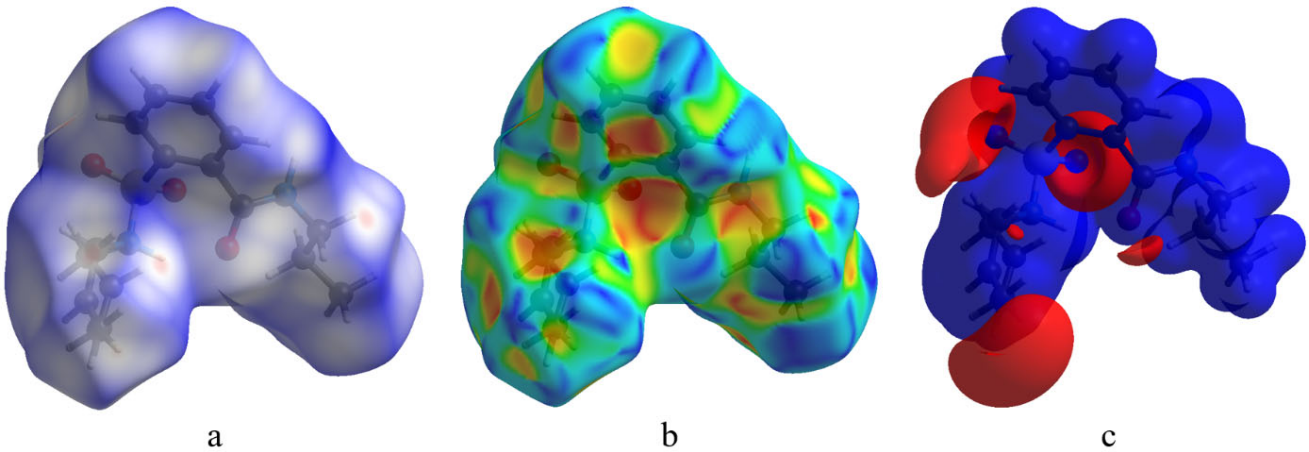

Figure 4. View of the Hirshfeld surface of 2-(*N*-allylsulfamoyl)-*N*-propylbenzamide. (**a**) Mapped over d_{norm} in the range of −0.4420 to 1.2928 a.u., (**b**) mapped over shape index. (**c**) Electrostatic potential energy in the range of −0.05 to 0.05 a.u., calculated using the STO-3 G basis set at the Hartree–Fock level of theory.

The three-dimensional d_{norm} surface shows the presence of several bright red spots which correspond to hydrogen bonding interactions, as shown in Figure 5.

The overall two-dimensional fingerprint plot [21] is shown in Figure 6a, while those delineated into H···H, H···O/O···H, H···C/C···H, H···N/N···H, C···O/O···C, O···O, N···O/O···N, O···O, and S···H/H···S contacts are illustrated in Figure 6b–g, respectively, together with their relative contributions to the Hirshfeld surface (HS). The most important interaction is H···H, contributing 59.2% to the overall crystal packing, which is reflected in Figure 6b as widely scattered points of high density due to the large hydrogen content of the molecule, with the tip at $d_e = d_i = 1.10$ Å. In the presence of O–H interactions, the pair of characteristic wings in the fingerprint plot delineated into H···O/O···H contacts (23.5% contribution to the HS), Figure 6c, has tips at $d_e + d_i = 2$ Å. The pair of scattered points of spikes in the fingerprint plot delineated into C···H/H···C, Figure 6d (14.6%), has tips at $d_e + d_i = 2.66$ Å. The N···H/H···N contacts, Figure 6e (1.6%), have tips at $d_e + d_i = 3.29$ Å. The O···C/C···O contacts, Figure 6f, contribute 0.6% to the HS and appear as a pair of scattered points of spikes with tips at $d_e + d_i = 3.17$ Å. The N···O/O···N contacts, Figure 6g, contribute 0.2% to the HS and appear as a pair of scattered points of spikes with tips at $d_e + d_i = 3.34$ Å. The O···O contacts, Figure 6h, contribute 0.2% to the HS and appear as a pair of scattered points of spikes with a tip at $d_e + d_i = 3.26$ Å. Finally, the S···H/H···S contacts, Figure 6i, make only a 0.1% contribution to the HS and have a low-density distribution of points.

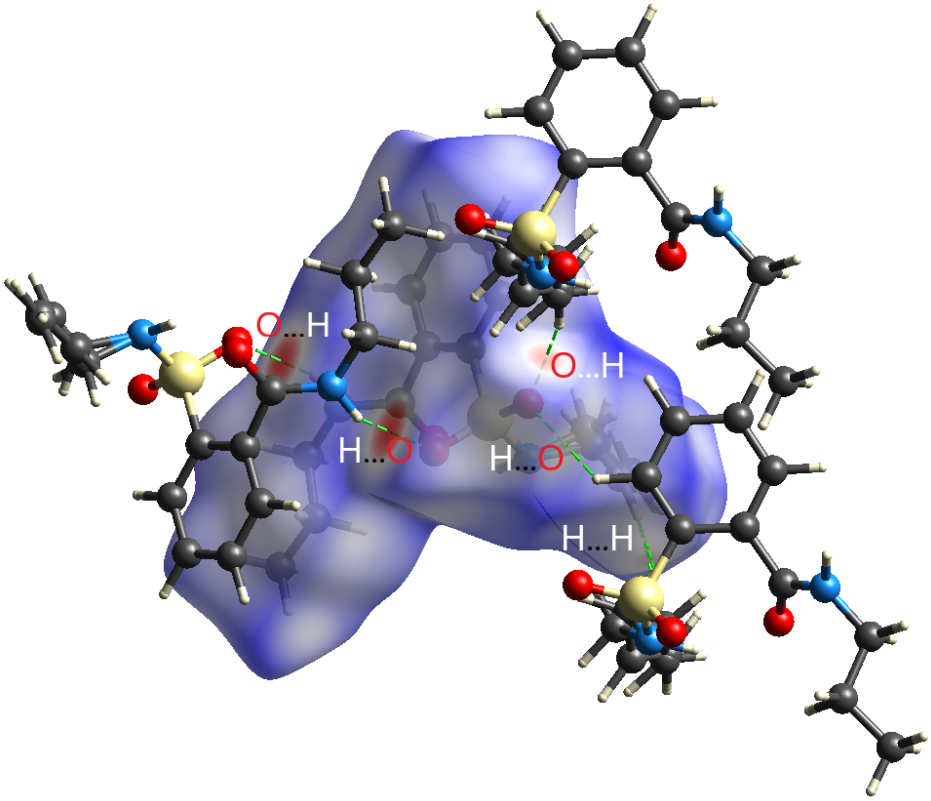

Figure 5. The Hirshfeld surface plotted over d_{norm} and the main non-covalent interactions in the crystal packing of 2-(*N*-allylsulfamoyl)-*N*-propylbenzamide.

2.3. Density Functional Theory Calculations

The structure in the gas phase of 2-(*N*-allylsulfamoyl)-*N*-propylbenzamide was optimized by means of density functional theory. The density functional theory calculation was performed by the hybrid B3LYP method and the 6–311 G(d,p) basis set, which is based on Becke's model [22] and considers a mixture of exact (Hartree–Fock) and density functional theory exchange using the B3 functional, together with the LYP correlation functional [23]. After obtaining the converged geometry, the harmonic vibrational frequencies were calculated at the same theoretical level to confirm that the number of imaginary frequencies is zero for the stationary point. Both the geometry optimization and harmonic vibrational frequency analysis of the title compound were performed with the GAUSSIAN 09 program [24]. As a result of these calculations, many quantum chemical parameters were found. Each parameter describes a different chemical property of a molecule [25]. The theoretical and experimental results related to bond lengths and angles are summarized in Table 2. Calculated numerical values for the title compound including electronegativity (χ), hardness (η), ionization potential (I), dipole moment (μ), electron affinity (A), electrophilicity (ω), and softness (σ) are collated in Table 3. Among the calculated parameters of the molecules, the highest occupied molecular orbital (HOMO) and lowest unoccupied molecular orbital (LUMO) parameters are more important than the others [26,27]. The electron transition from the HOMO to the LUMO energy level is shown in Figure 7. The green and brown regions of the figure represent molecular orbitals with completely opposite phases. The positive phase of the molecule is shown in green and the negative phase in brown. The HOMO and LUMO are localized in the plane extending over the whole 2-(*N*-allylsulfamoyl)-*N*-propylbenzamide system. The energy band gap [ΔE = ELUMO-EHOMO] of the molecule is 5.3828 eV, and the frontier molecular orbital energies, EHOMO and ELUMO, are −6.9656 and −1.5828 eV, respectively.

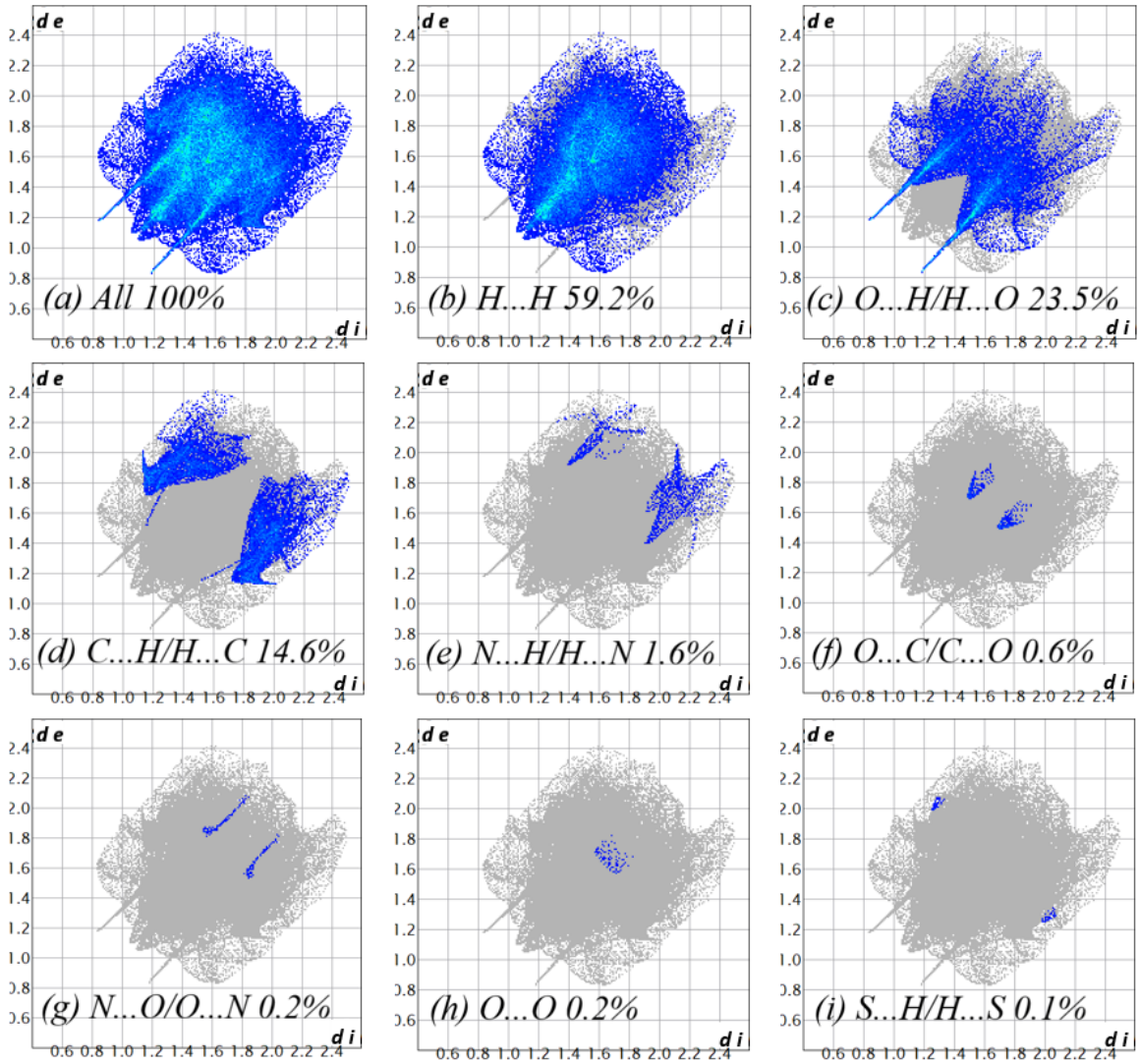

Figure 6. Two-dimensional fingerprint plots for the title compound showing (**a**) all interactions, and delineated into (**b**) H···H, (**c**) H···O/O···H, (**d**) C···H/H···C, (**e**) N···H/H···N, (**f**) O···C/C···O, (**g**) N···O/O···N, (**h**) O···O, and (**i**) S···H/H···S interactions. The d_i and d_e values are the closest internal and external distances (in Å) from given points on the Hirshfeld surface.

Table 3. Calculated energies.

Molecular Energy	Title Compound
Total energy TE (eV)	−33,735.8573
E_{HOMO} (eV)	−6.9656
E_{LUMO} (eV)	−1.5828
Gap, ΔE (eV)	5.3828
Dipole moment, μ (Debye)	4.6564
Ionization potential, I (eV)	6.9656
Electron affinity, A	1.5828
Electronegativity, χ	4.2742
Hardness, η	2.6914
Electrophilicity index ω	3.3939
Softness, σ	0.3716
Fraction of electron transferred, ΔN	0.5064

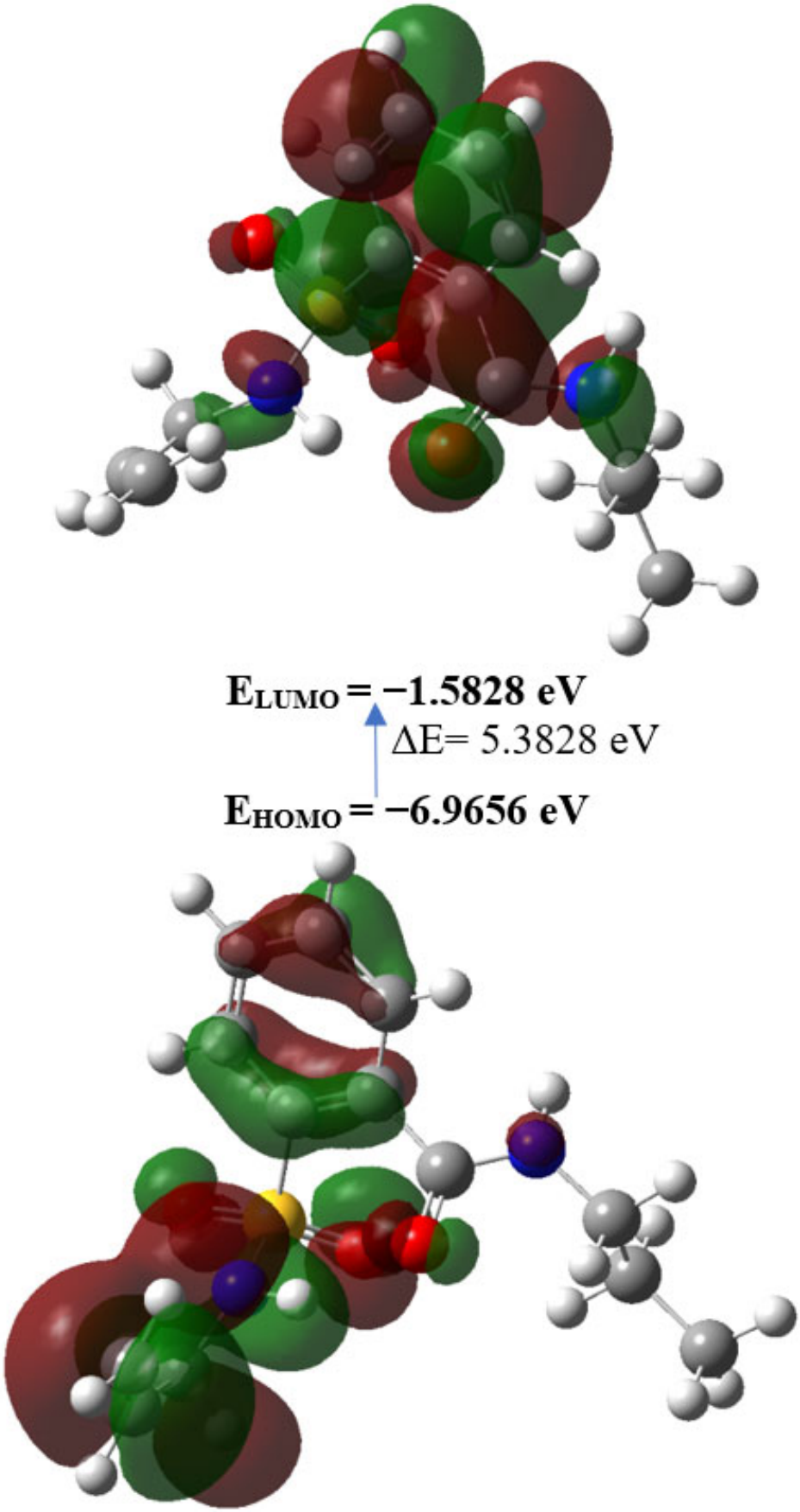

Figure 7. The energy band gap of 2-(*N*-allylsulfamoyl)-*N*-propylbenzamide.

3. Experimental Section

3.1. Materials and Methods

NMR spectra were recorded on a Bruker AC 200 spectrometer (Bruker Biospin, Rheinstetten, Germany) at 200 MHz for ^{1}H NMR and 50 MHz for ^{13}C NMR in dry $CDCl_3$ solvent. Mass spectral analyses (ESI-MS) were recorded on an Agilent Technologies 1260 Infinity II LC/MSD (Agilent Technologies, Santa Clara, CA, USA) and the samples were diluted in acetonitrile. Melting points were determined on a Munz Köfler Bench System. Analytical thin-layer chromatography (TLC) was performed on precoated with silica gel 60 GF254 (Merck, Darmstadt, Germany) and visualization was performed using a UV lamp at 254 and 360 nm. Ultrasound-assisted reactions were performed in a Vibra-Cell™ Model 75022 Ultrasonic Processor (Sonics & Materials Inc., Newtown, CT, USA) using a 4 mm titanium alloy Ti-6Al 4V probe (20 kHz, 130 W) with a 4 mm tip diameter. The reactions were performed at 60% P_{max} using a 10–50 mL pear-shaped flask with the sonotrode immersed in the solution for maximum energy.

3.2. Synthesis of Compound **4**

In a pear-shaped flask, a mixture of saccharin **1** (1 mmol), allyl bromide **2** (1.1 mmol), and K_2CO_3 (1.2 mmol) in H_2O (8 mL) was sonicated at 25 °C for 4 min using the ultrasonic probe. After completion of the reaction (monitored by TLC), a propylamine solution (2 mmol) was added. After sonication for 2 min, the crude mixture was filtered and the filtrate was extracted with CH_2Cl_2 (10 mL × 3). The organic phase was washed with saturated brine solution (10 mL × 2) and water (15 mL), dried over $MgSO_4$, and concentrated under vacuum. The residue was purified by recrystallization from EtOH to give pure single crystals of 2-(*N*-allylsulfamoyl)-*N*-propylbenzamide **4**.

White crystals, yield 94%, m.p. 125–127 °C (EtOH), TLC (cyclohexane/AcOEt, 6/4, *v*/*v*) Rf = 0.70; FTIR (ATR, cm^{-1}): 1645 (C=O), 3385 (NH_{amidic}); ^{1}H NMR (200 MHz, Chloroform-d) δ 7.93–7.83 (m, 1H, $1H_{Ar}$), 7.63–7.42 (m, 3H, $2H_{Ar}$, 1NH), 6.44–6.23 (m, 2H, 1NH, $1H_{Ar}$), 5.81–5.56 (m, 1H, $H_{allylic}$),), 5.15 (dd, J = 17.1, 1.5 Hz, 1H, $H_{allylic}$),), 5.03 (dd, J = 10.2, 1.4 Hz, ^{1}H, $H_{allylic}$), 3.55 (m, J = 5.9, 1.5 Hz, 2H, N-CH_2), 3.37 (q, J = 6.1 Hz, 2H, CH_2), 1.77–1.54 (m, 2H, CH_2), 0.99 (t, J = 7.4 Hz, 3H, CH_3). 13C NMR (50 MHz, $CDCl_3$) δ 169.5 (C=O), 137.9 (C-S), 135.5, 132.9, 132.5, 130.0, 129.3, 128.3, 117.3, 46.2(C-$NH_{sulfonamidic}$), 42.1 (C-NH_{amidic}), 22.5 (CH_2), 11.4 (CH_3); MS (ESI+): m/z = 283.0 $[M + H]^+$.

The Figures S1–S4 containing 1H, 13C NMR, mass, and IR spectra of the synthesized compound **4**.

3.3. X-ray Data of Crystal Structure

Crystal data, data collection, and structure refinement details are given in Table 4. Refinement of F^2 against ALL reflections. H atoms attached to carbon were placed in calculated positions (C—H = 0.95–0.99 Å) and were included as riding contributions with isotropic displacement parameters 1.2–1.5 times those of the attached atoms. Those attached to nitrogen were placed in locations derived from a difference map and refined independently. The allyl group is disordered over two sites in a 0.920 (3)/0.080 (3) refined ratio and the components were refined with SAME, SADI, and EADP restraints so that their geometries and displacement parameters would be comparable.

Table 4. Experimental details.

Crystal Data	
Empirical formula	$C_{13}H_{18}N_2O_3S$
Formula weight	282.35
Temperature/K	150
Crystal system, space group	Monoclinic, $P2_1/c$

Table 4. *Cont.*

Crystal Data	
a, b, c (Å)	8.2659 (3), 21.4034 (8), 8.3357 (3)
β (°)	106.366 (1)
Volume (Å^3)	1414.98 (9)
Z	4
Radiation type	Cu Kα
μ (mm^{-1})	2.09
Crystal size (mm)	0.23 × 0.13 × 0.13
Data collection	
Diffractometer	Bruker D8 Venture Photon 3 CPAD
Absorption correction	Multi-scan SadabsBruker, (Bruker, Karlsruher, Germany) [28]
T_{min}, T_{max}	0.72, 0.78
No. of measured, independent, and observed [$I > 2\sigma(I)$] reflections	44,247, 2834, 2811
R_{int}	0.024
(sin θ/λ)max (Å^{-1})	0.625
Refinement	
$R[F^2 > 2\sigma(F^2)]$, $wR(F^2)$, S	0.029, 0.075, 1.04
No. of reflections	2834
No. of parameters	191
No. of restraints	4
H atom treatment	H atoms treated by a mixture of independent and constrained refinement
Δρmax, Δρmin (e Å^{-3})	0.37, −0.33

Computer programs: APEX4 [15], SAINT [15], SHELXT [16], SHELXL [17], DIAMOND [29], SHELXTL [15].

4. Conclusions

A new heterocycle containing allylsulfamoyl and propylbenzamide moieties has been synthesized. The procedure used was simple and the yield obtained was high. Nuclear magnetic resonance and X-ray diffraction were used to establish the structure of the newly synthesized heterocycle. The intra- and inter-molecular interactions have been elaborated via the study of the Hirshfeld surface and a comparative theoretical study has also been described.

Supplementary Materials: The following supporting materials, containing ^{1}H, ^{13}C NMR, mass, and IR spectra (see Supplementary Materials Figures S1–S4) of the synthesized compound **4** can be downloaded online.

Author Contributions: Conceptualization, methodology, writing—original draft preparation, K.B, L.M. and A.E.m.; X-ray crystallography experiments and structural comparisons by J.T.M.; Hirshfeld surface analysis and spectroscopic studies were performed by K.C.; investigation, writing—review and editing, K.B. All authors have read and agreed to the published version of the manuscript.

Funding: This research received no external funding.

Data Availability Statement: Not applicable.

Acknowledgments: This work is supported by UM5R. The authors thank UATRS-CNRST Morocco.

Conflicts of Interest: The authors declare no conflict of interest.

References

1. Mustafa, M.; Winum, J.Y. The importance of sulfur-containing motifs in drug design and discovery. *Expert Opin. Drug Discov.* **2022**, *17*, 501. [CrossRef]
2. Giovannuzzi, S.; D'Ambrosio, M.; Luceri, C.; Osman, S.M.; Pallecchi, M.; Bartolucci, G.; Nocentini, A.; Supuran, C.T. Aromatic sulfonamides including a sulfonic acid tail: New membrane impermeant carbonic anhydrase inhibitors for targeting selectively the cancer-associated isoforms. *Int. J. Mol. Sci.* **2022**, *23*, 461. [CrossRef]

3. Ferraroni, M.; Angeli, A.; Pinteala, M.; Supuran, C.T. Sulfonamide diuretic azosemide as an efficient carbonic anhydrase inhibitor. *J. Mol. Struct.* **2022**, *1268*, 133672. [CrossRef]
4. Rubab, L.; Afroz, S.; Ahmad, S.; Hussain, S.; Nawaz, I.; Irfan, A.; Batool, F.; Kotwica-Mojzych, K.; Mojzych, M. An update on synthesis of coumarin sulfonamides as enzyme inhibitors and anticancer agents. *Molecules* **2022**, *27*, 1604. [CrossRef] [PubMed]
5. Ghomashi, R.; Ghomashi, S.; Aghaei, H.; Massah, A.R. Recent Advances in Biological Active Sulfonamide based Hybrid Compounds Part A: Two-Component Sulfonamide Hybrids. *Curr. Med. Chem.* **2023**, *30*, 407. [PubMed]
6. Moskalik, M.Y. Sulfonamides with Heterocyclic Periphery as Antiviral Agents. *Molecules* **2023**, *28*, 51. [CrossRef]
7. Deng, Z.; Sun, H.; Bheemanaboina, R.R.Y.; Luo, Y.; Zhou, C.H. Natural aloe emodin-hybridized sulfonamide aminophosphates as novel potential membrane-perturbing and DNA-intercalating agents against Enterococcus faecalis. *Bioorg. Med. Chem.* **2022**, *64*, 128695. [CrossRef]
8. Portela, M.B.; Barboza, C.M.; da Silva, E.M.; de Moraes, D.C.; Simão, R.A.; de Souza, C.R.; Da Silva Cardoso, V.; Ferreria-Pereria, A.; Vermelho, A.B.; Supuran, C.T. Dentine biomodification by sulphonamides pre-treatment: Bond strength, proteolytic inhibition, and antimicrobial activity. *J. Enzym. Inhib. Med. Chem.* **2023**, *38*, 319. [CrossRef]
9. Köksal, Z.; Kalin, R.; Camadan, Y.; Usanmaz, H.; Almaz, Z.; Gülçin, I.; Gokcen, T.; Ceyhan Goren, A.; Ozdemir, H. Secondary sulfonamides as effective lactoperoxidase inhibitors. *Molecules* **2017**, *22*, 793. [CrossRef]
10. Azevedo-Barbosa, H.; Dias, D.F.; Franco, L.L.; Hawkes, J.A.; Carvalho, D.T. From antibacterial to antitumour agents: A brief review on the chemical and medicinal aspects of sulfonamides. *Mini-Rev. Med. Chem.* **2020**, *20*, 2052–2066. [CrossRef]
11. Mondal, S.; Malakar, S. Synthesis of sulfonamide and their synthetic and therapeutic applications: Recent advances. *Tetrahedron* **2020**, *76*, 131662. [CrossRef]
12. EL Mahmoudi, A.; Tachallait, H.; Moutaoukil, Z.; Arshad, S.; Karrouchi, K.; Benhida, R.; Bougrin, K. Ultrasound-Assisted Green Synthesis of 3, 5-Disubstituted Isoxazole Secondary Sulfonamides via One-Pot Five-Component Reaction using $CaCl_2/K_2CO_3$ as Pre-Catalyst in Water. *ChemistrySelect* **2022**, *7*, e202203072. [CrossRef]
13. El Mahmoudi, A.; El Masaoudi, H.; Tachallait, H.; Talha, A.; Arshad, S.; Benhida, R.; Jaber, B.; Benaissa, M.; Bougrin, K. Selective silver (I)-catalyzed four-component gram-scale synthesis of novel 1,4-disubstituted 1,2,3-triazole-sulfonamides under heterogeneous catalysis and microwave irradiation in water. *Results Chem.* **2022**, *4*, 100552. [CrossRef]
14. El Mahmoudi, A.; Chkirate, K.; Tachallait, H.; Van Meervelt, L.; Bougrin, K. 2-((3-(4-Methoxyphenyl)-4,5-dihydroisoxazol-5-yl)methyl)benzo[d]isothiazol-3(2H)-one1,1-dioxide. *Molbank* **2022**, *2022*, M1488. [CrossRef]
15. Bruker. *APEX4, SAINT & SHELXTL*; Bruker AXS LLC: Madison, WI, USA, 2021.
16. Sheldrick, G.M. SHELXT—Integrated space-group and crystal-structure determination. *Acta Cryst. A* **2015**, *71*, 3. [CrossRef]
17. Sheldrick, G.M. Crystal structure refinement with SHELXL. *Acta Cryst. C* **2015**, *71*, 3–8. [CrossRef]
18. Hirshfeld, F.L. Bonded-atom fragments for describing molecular charge densities. *Theor. Chim. Acta* **1977**, *44*, 129. [CrossRef]
19. Spackman, M.A.; Jayatilaka, D. Hirshfeld surface analysis. *Cryst. Eng. Comm.* **2009**, *11*, 19. [CrossRef]
20. Turner, M.J.; McKinnon, J.J.; Wolff, S.K.; Grimwood, D.J.; Spackman, P.R.; Jayatilaka, D.; Spackman, M.A. *CrystalExplorer17*; The University of Western Australia: Crawley, Australia, 2017.
21. McKinnon, J.J.; Jayatilaka, D.; Spackman, M.A. Towards quantitative analysis of intermolecular interactions with Hirshfeld surfaces. *Chem. Commun.* **2007**, *37*, 3814. [CrossRef] [PubMed]
22. Becke, A.D. Density-functional thermochemistry. III. The role of exact exchange. *J. Chem. Phys.* **1993**, *98*, 5648–5652. [CrossRef]
23. Lee, C.; Yang, W.; Parr, R.G. Development of the Colle-Salvetti correlation-energy formula into a functional of the electron density. *Phys. Rev. B* **1988**, *37*, 785. [CrossRef]
24. Frisch, M.J.; Trucks, G.W.; Schlegel, H.B.; Scuseria, G.E.; Robb, M.A.; Cheeseman, J.R.; Scalmani, G.; Barone, V.; Mennucci, B.; Petersson, G.A.; et al. *GAUSSIAN09, Revision A.02*; Gaussian Inc.: Wallingford, CT, USA, 2009.
25. Chkirate, K.; Azgaou, K.; Elmsellem, H.; El Ibrahimi, B.; Sebbar, N.K.; Anouar, E.H.; Benmessaoud, M.; El Hajjaji, S.; Essassi, E.M. Corrosion Inhibition Potential of 2-[(5-methylpyrazol-3-yl)methyl]benzimidazole against carbon steel corrosion in 1M HCl solution: Combining Experimental and Theoretical Studies. *J. Mol. Liq.* **2021**, *321*, 114750. [CrossRef]
26. Bouzian, Y.; Sert, Y.; Karrouchi, K.; Van Meervelt, L.; Chkirate, K.; Mahi, L.; Hamou Ahabchane, N.; Talbaoui, A.; Essassi, E.M. Synthesis, spectroscopic characterization, DFT, molecular docking and in vitro antibacterial potential of novel quinoline derivatives. *J. Mol. Struct.* **2021**, *1246*, 131217. [CrossRef]
27. Chkirate, K.; Akachar, J.; Hni, B.; Hökelek, T.; Anouar, E.H.; Talbaoui, A.; Mague, J.T.; Sebbar, N.K.; Ibrahimi, A.; Essassi, E.M. Synthesis, spectroscopic characterization, crystal structure, DFT, ESI-MS studies, molecular docking and in vitro antibacterial activity of 1,5-benzodiazepin-2-one derivatives. *J. Mol. Struct.* **2022**, *1247*, 131188. [CrossRef]
28. Krause, L.; Herbst-Irmer, R.; Sheldrick, G.M.; Stalke, D. Comparison of silver and molybdenum microfocus X-ray sources for single-crystal structure determination. *J. Appl. Cryst.* **2015**, *48*, 3. [CrossRef]
29. Brandenburg, K.; Putz, H. *DIAMOND*; Crystal Impact GbR: Bonn, Germany, 2012.